Investigating Hydrodynamics and Circulation in the Gullmar Fjord

Implementation and configuration of the Versatile Ocean Simulator (Veros)

Bachelor thesis

Written by *Maria Friis Greibe*

January 13, 2025

Supervised by

Markus Jochum

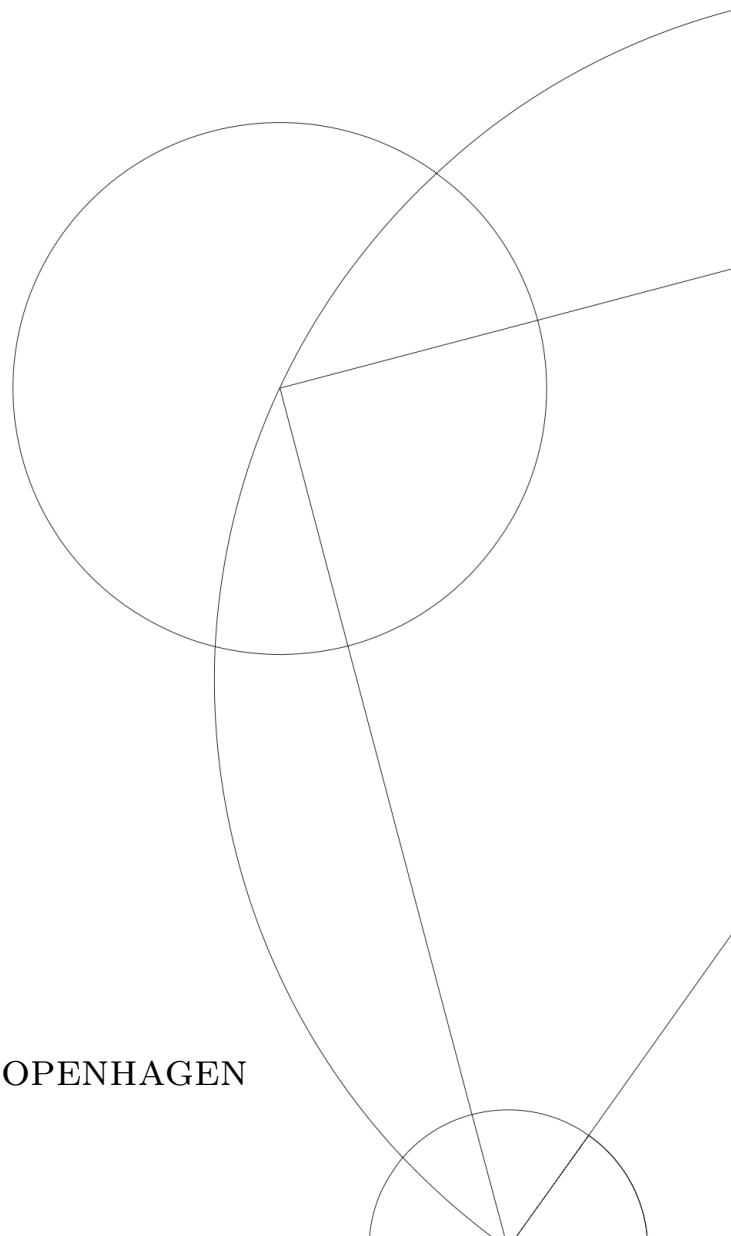

University of Copenhagen

UNIVERSITY OF COPENHAGEN

Name of Institute:	Niels Bohr Institute
Name of Department:	TeamOcean
Author(s):	Maria Friis Greibe
Email:	rkq216@alumni.ku.dk
Title and subtitle:	Investigating Hydrodynamics and Circulation in the Gullmar Fjord - Implementation and configuration of the Versatile Ocean Simulator (Veros)
Supervisor(s):	Markus Jochum
Handed in:	13.01.2025
Defended:	23.01.2025

Name _____ Name _____

Signature _____ Signature _____

Date _____ Date _____

Abstract

Fjords are critical links between land and ocean, sensitive to both climate change and human impacts, making it essential to understand their dynamics. In this thesis, a numerical model of the Gullmar fjord was set up using the *Versatile Ocean Simulator* (Veros) to investigate its hydrodynamics and circulation. The model was discretized with a horizontal resolution of 93 m $\times$ 97 m and a vertical resolution of 5 m. Various parameters in the numerical scheme in Veros were tuned to minimize the numerical noise, with increased horizontal viscosity, isoneutral diffusivity, and the use of no-slip boundary conditions resulting in the least noise. The optimized model was tested for five different cases, where different types of circulation were forced, and then compared with the theory on fjord circulation. It was possible to force estuarine circulation, which is driven by freshwater supply, and estimate the resulting transport with Knudsen's relations, both in the case of no wind, in the case of added oscillating wind, and in the case of forced intermediary circulation. It was also possible to force basin water renewal and intermediary circulation, which is driven by variations of the density in the coastal water. The intermediary circulation in the model was compared with an empirical formula for intermediary exchange, with the formula resulting in higher transport than the model transport throughout the fjord. The results of the five cases demonstrate that the Gullmar fjord model, configured in Veros, can simulate circulations consistent with the existing theory on fjords. Future improvements of the model include the implementation of open boundaries at the fjord mouth to reduce unwanted reflections and mixing, as well as smoothing of the bathymetry to further minimize noise.

Contents

1 Introduction

Fjords serve as important interfaces between land and open ocean, extending the transition between the two, resulting in large gradients and stratified circulations [5]. They play an essential part in the biochemical cycle, for instance it is estimated that they bury 11 % of the global oceanic organic carbon [19]. Fjords are also very sensitive to human impact, such as eutrophication, fishery, or pollution, as well as to climate change, which can impact fjords through changed temperature, wind forcing, or sea level [17]. It is therefore important to understand the hydrodynamics and circulation of fjords.

Numerical modelling of fjords is a great tool to understand the dynamics of fjords and explore how fjords may change by impacts of humans and climate change. A number of different coastal ocean models already exist [17]. The goal of this project is to set up a model of the Gullmar fjord using the *Versatile Ocean Simulator* (Veros). The advantage of Veros is that it is written in pure Python and is thus easy to access, use and modify. Veros provides a range of pre-configured model setups, including an ACC channel model and global models in different resolutions [14]. However, it has yet to be configured for a smaller model domain, such as the Gullmar fjord. Consequently, configuring Veros for the Gullmar fjord requires tuning of several parameters to ensure numerical stability and minimize noise. The model solution will be analyzed under different forcings and compared with existing theory on circulation of fjords.

This thesis is structured as follows: Section 2 introduces the theory about the circulation of fjords. Section 3 lays out a description of ocean modelling and Veros. Section 4 outlines the methods used to configure the Gullmar fjord model. Finally, Section 5 presents an analysis and discussion of the model results.

2 Circulation of fjords

Fjords are semi-enclosed coastal inlets carved by glacial processes and most fjords have a sill at the mouth and river discharge into the head. The mouth and head of the fjord are used to describe the fjords opening to the coastal sea and the fjords inland end, respectively. A sill is a rise in the bathymetry often located near the mouth [9]. A basic sketch of a fjord is presented in Figure 1. The fjord water can approximately be partitioned into three different water masses: the *surface water*, which has low salinity due to freshwater supply from river discharge and precipitation, the *intermediary water*, which lies beneath the surface water and above the sill level, and the *basin water*, which is the densest water and is located below sill level. The surface water and the intermediary water have free connection with the coastal waters, while the basin water does not. This results in the basin water being mostly stagnant and only renewed when the density of the coastal water at sill level exceeds the density of the basin water [20]. The circulation of fjords is forced by freshwater input, winds, tides and changes in sea level and stratification of the coastal water [20]. A difference in sea level inside and outside the fjord gives rise to a horizontal barotropic pressure gradient. Differences in stratification give rise to horizontal baroclinic pressure gradients and are a result of freshwater supply and variations in coastal waters stratification at the mouth [15].

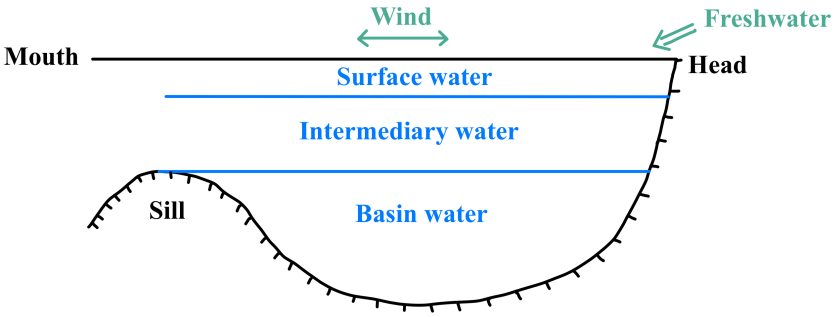

Figure 1: Sketch of water masses and circulation in a sill fjord. The sketch is inspired by a similar sketch in "Hydrodynamics and circulation of fjords" [20].

In this project the main focus is the baroclinic driven circulation, and the barotropic flow will not be discussed further. In the following two sections, two different baroclinic driven circulations are presented; the *estuarine circulation*, forced by freshwater supply, and the *intermediary circulation*, forced by density variations in coastal water. Following the descriptions of the two circulations, a short overview of knowledge of the circulation in the Gullmar fjord is presented.

2.1 Estuarine circulation

The estuarine circulation is a baroclinic circulation, driven by freshwater supply inside the fjord from river discharge and precipitation. The freshwater supply forms the surface water layer, which due to the horizontal pressure gradient will flow out of the fjord, and in turn, coastal water will flow into the fjord beneath the outflowing surface layer. It is this circulation of an outflowing brackish surface layer and a more saline inflowing layer which is termed the estuarine circulation [20].

2.1.1 Knudsen's relations

Knudsen's relations quantify the inflow and outflow in the estuarine circulation and are derived from the principles of volume and salt mass conservation in the fjord [6]. Figure 2 provides sketches of the layers and transects in the fjord, as well as a visualization of the notation used in the derivation. Let Q^i_{out} and Q^i_{in} denote the time averaged volume fluxes for the outgoing

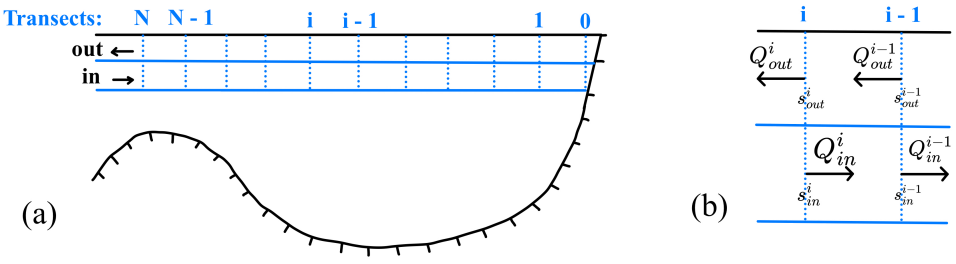

Figure 2: (a) sketch of the fjord, showing the two layers and the defined transects used in the derivation of Knudsen's relations. (b) example of notations for the transport and salinity at transect i and $i-1$

upper layer and the ingoing lower layer at transect i with the representative salinities s^i_{out} and

s^i_{in}. Assuming steady state and incompressibility and neglecting turbulent transport, volume conservation in the volume enclosed by the transects i and $i-1$ can be written as [6]:

$$Q^i_{in} + Q^{i-1}_{out} - Q^i_{out} - Q^{i-1}_{in} = 0 \tag{1}$$

and the salt conservation equation can be formulated as [6]:

$$Q^i_{out} s^i_{out} - Q^i_{in} s^i_{in} = Q^{i-1}_{out} s^{i-1}_{out} - Q^{i-1}_{in} s^{i-1}_{in} = 0 \tag{2}$$

Equation (1) and (2) constitute two equations with four unknowns and can thus be solved if the volume transports at one of the transects are known. Suppose that the transports are known at transect $i-1$, then the two equations can be solved for the two unknown transports:

$$Q^i_{out} = Q^{i-1}_{out} \frac{s^i_{in}}{s^{i-1}_{in}} \frac{s^{i-1}_{in} - s^{i-1}_{out}}{s^i_{in} - s^i_{out}} \quad Q^i_{in} = Q^{i-1}_{in} \frac{s^i_{out}}{s^{i-1}_{out}} \frac{s^{i-1}_{in} - s^{i-1}_{out}}{s^i_{in} - s^i_{out}} \tag{3}$$

These are Knudsen's relations and can be used to calculate the volume fluxes in the estuarine circulation using only salinity data for the two layers and the volume transports at one location, as these equations are an iterative scheme. If, for simplicity, it is assumed that all freshwater supply to the fjord happens by river discharge at the fjord head, then at transect $i = 0$: $Q^0_{out} = F$ and $s^0_{out} = 0$, with F being the freshwater flux. There is no ingoing layer at the mouth, but Q^1_{in} must be equal to the volume transport necessary to increase the transport at transect $i = 1$ from F to Q^1_{out}, so the initial conditions for the iteration scheme are:

$$Q^1_{out} = F \frac{s^1_{in}}{s^1_{in} - s^1_{out}} \quad Q^1_{in} = Q^1_{out} - F \tag{4}$$

So by using Knudsen's relations, equation (3), and given the freshwater supply and the initial conditions in equation (4), the volume transport at every transect with measured salinities of the two layers in the fjord can be estimated. Since Knudsen's relations use actual salinities (either measured or modeled), the estimated transports are not necessarily only due to the estuarine circulation but are a result of all forcing. In the derivation of the Knudsen relations, turbulent transport was assumed negligible, and thus the Knudsen's relations can't be used to estimate the transports in regions, where turbulent mixing can't be neglected. It can additionally be observed in equation (3) that as the salinity difference between the two layers decreases, the transport increases, and as the salinity difference approaches zero, the transport will diverge. This means that the relations are best applied to sections of the fjord away from sills and rivers, where more mixing occurs, and in sections where the vertical stratification is strong [7].

2.2 Intermediary circulation

The intermediary circulation is driven by horizontal pressure gradients between the fjord water and the coastal water. These horizontal pressure gradients are a result of density variations in the coastal waters and drive currents, that adjust the stratification inside the fjord to the stratification outside it [20]. By using a numerical model and series of density observations, an empirical formula for the intermediary circulation has been derived in Stigebrandt and Aure (1990):

$$Q_i = \gamma \left(g B_m H_t A_f \frac{\Delta M}{\rho_0} \right)^{1/2} \tag{5}$$

where Q_i is the long term average magnitude of the ingoing and outgoing volume fluxes caused by the intermediary circulation, $\gamma = 17 \cdot 10^{-4}$ is a dimensionless empirical coefficient estimated for Scandinavian conditions, B_m is the width of the mouth, H_t is the sill depth, A_f is the horizontal area of the surface of the fjord, ρ_0 is a reference density and ΔM is the vertical integral of the standard deviation of the density, $\sigma_\rho(z)$, at the mouth [20]:

$$\Delta M = \int_0^{H_t} \sigma_\rho(z) dz \tag{6}$$

Aure et al. (1996) suggest that ΔM should be dependent on the frequencies of the density variations and Arneborg (2004) found that higher frequencies are most important for the intermediary circulation in the Gullmar fjord [20]. If it is assumed that the amplitude of vertical motion is the same in the whole fjord, the intermediary transport at a distance y from the mouth is:

$$Q_i(y) = Q_i \frac{A(y)}{A_f} \tag{7}$$

where $A(y)$ is the horizontal surface area of the fjord between the head and the distance y from the mouth. This equation doesn't include damping of intermediary circulation with increasing distance to the mouth, which has been observed in the Gullmar fjord [20]. So equation (5) and equation (7) give an estimate of the transport due to the intermediary circulation, but don't accommodate for the damping of the intermediary circulation and the frequency dependency of ΔM.

2.3 The Gullmar fjord

The Gullmar fjord is located on the west coast of Sweden, is 28 km long and its width is between 1 and 2 km. The Gullmar fjord has a sill depth of 43 m and a maximum depth of approximately 120 m [4], see Figure 3. The main freshwater supply to the fjord comes from the Örekil river, which is located at the head of the fjord, which, averaged over long time, discharge $21 m^3/s$ freshwater. When considering the precipitation area of the Gullmar fjord, the total freshwater supply to the fjord is $25 m^3/s$ [21]. The fjord is characterized by weak tides with amplitudes below $0.2m$ and the basin water below $50m - 60m$ is stagnant most of the year and is renewed during the winter [4]. Vertical variations of the stratification in the coastal water are shown to be the main mechanism of water exchange above sill level, and the intermediary circulation is thus much more dominant than the estuarine circulation [1].

3 Ocean modelling

In the following section, the ocean model Veros, its governing equations and some of the parametrizations it offers are presented. Additionally, differences between small and large scale ocean modelling are highlighted.

3.1 Veros

Veros (the versatile ocean simulator) is a numerical ocean model written purely in Python [14]. Veros is a translation of pyOM2 (Python Ocean Model), which has a Fortran backend and a

Python front end [8]. Veros solves the semi-compressible, hydrostatic, Boussinesq primitive equations, described in the next section, using finite differences on an Arakawa C-grid and supports both cartesian and pseudo-spherical coordinates [13]. The Arakawa C-grid is a structured, scattered grid where tracers, meridional, zonal, and vertical velocities are calculated on different grids. An Adam-Bashforth second order time stepping scheme is used to integrate the momentum equation [8].

3.2 The model equations

The Navier-Stokes equations in a rotating reference frame is given by the momentum equation:

$$\frac{D\mathbf{u}}{Dt} + 2\mathbf{\Omega} \times \mathbf{u} = -\frac{1}{\rho}\nabla p - \nabla\phi + \mathcal{F} \tag{8}$$

where $\mathbf{u} = (u, v, w)$ is the velocity field, $\mathbf{\Omega}$ is the angular velocity of the earths rotation, ρ is the density of the fluid, p is the pressure, $\phi = gz$ is the geo potential and $\mathcal{F}$ is the dissipation of momentum [18]. When applying the hydrostatic approximations, which balance the gravitational term with the pressure gradient, and the Boussinesq approximations, which exploit the small variation of density in the ocean, equation (8) takes the form:

$$\frac{D\mathbf{u_h}}{Dt} + f\hat{\mathbf{k}} \times \mathbf{u_h} = -\frac{1}{\rho_0}\nabla_h p' + \mathcal{F} \tag{9a}$$

$$\frac{\partial p'}{\partial z} = -\rho' g \tag{9b}$$

with $\mathbf{u_h}$ being the horizontal velocity, ρ_0 a fixed reference density, ρ' the perturbation density, p' the dynamic pressure and f the coriolis frequency. Together with the continuity equation; $\nabla_h \cdot \mathbf{u_h} + \frac{\partial w}{\partial z} = 0$, the tracer equations and the equations of state, equation (9) constitutes the primitive equations, which are the governing equations that most ocean circulation models solve, including Veros [13].

3.3 The turbulence closure problem

The flow in the oceans consists of fluctuations within a wide range of length scales. To be able to resolve fluctuations with a specific length scale, a numerical ocean model must have a spatial grid scale on the order of the length scale of the fluctuations. This means that in order to resolve the smallest fluctuations, the model will require a very high resolution, which is not computationally possible. Therefore, it is relevant to describe the mean flow by time-averaging the Navier-Stokes equations. This is done by separating the flow quantities into a mean part and a fluctuating part and then averaging the equations of motion, a method called Reynolds averaging [22].

Reynolds averaging of the momentum equations results in additional terms written in Einstein notation as: $\frac{\partial}{\partial x_j}(-\overline{u_j' u_i'})$, where primes denote the fluctuations and time averaged are denoted by an overbar. $-\overline{u_j' u_i'}$ is called the Reynolds stress and can be described as the average stress the fluctuations exert on the mean flow. This introduces the problem known as the turbulence closure problem; the Reynold averaged Navier-Stokes equations have more unknowns than equations, and thus all fluctuations smaller than the grid length scale in an ocean model will impact the

flow in a way that can't be predicted [18]. To close the system, the Reynolds stresses are parameterized by relating the fluctuations to the mean quantities [10]:

$$-\overline{\mathbf{u_h}'u'} = \kappa_h \frac{\partial \overline{\mathbf{u_h}}}{\partial x} \quad -\overline{\mathbf{u_h}'v'} = \kappa_h \frac{\partial \overline{\mathbf{u_h}}}{\partial y} \quad -\overline{\mathbf{u_h}'w'} = \kappa_v \frac{\partial \overline{\mathbf{u_h}}}{\partial z} \tag{10}$$

with a separation of the vertical and horizontal turbulent viscosity, κ_v and κ_h. Because the turbulent viscosity are several orders of magnitude larger than the molecular viscosity, the molecular viscosity can be neglected and the dissipation of momentum in equation (9) can therefore be defined by the turbulent viscosity as [18]:

$$\mathcal{F} = \nabla_h \cdot (\kappa_h \nabla_h \mathbf{u_h}) + \frac{\partial}{\partial z}(\kappa_v \frac{\partial \mathbf{u_h}}{\partial z}) \tag{11}$$

where the horizontal and vertical viscosity either can be given as constant or can be parameterized by a scheme. The same parametrization can be made for the turbulent diffusivity [10].

3.3.1 Turbulent kinetic energy closure scheme

To parameterize the vertical turbulent viscosity and diffusivity, Veros offers the turbulent kinetic energy, TKE, closure scheme. The TKE closure scheme is a second order turbulence closure scheme used in many ocean models, where the vertical viscosity is related to the turbulent kinetic energy as:

$$\kappa_m = c_k l_k \sqrt{\bar{e}} \tag{12}$$

where κ_m is the vertical viscosity, c_k is a mixing coefficient, l_k is the mixing length scale and $\bar{e} = \frac{1}{2}(u'^2 + v'^2 + w'^2)$ is the turbulent kinetic energy [10]. The TKE budget equation is [10]:

$$\frac{\partial \bar{e}}{\partial t} = \frac{\partial}{\partial z}\left(\kappa_e \frac{\partial \bar{e}}{\partial z}\right) + \kappa_m \left(\left(\frac{\partial \bar{u}}{\partial z}\right)^2 + \left(\frac{\partial \bar{v}}{\partial z}\right)^2\right) - \kappa_h N^2 - c_\varepsilon \frac{\bar{e}^{3/2}}{l_\varepsilon} \tag{13}$$

where $\kappa_e = \alpha_{tke}\kappa_m$ is the vertical diffusive flux of TKE, $\kappa_h = \frac{\kappa_m}{P_{rt}}$ is the vertical turbulent diffusivity of tracers, N^2 is the buoyancy frequency and c_ε and l_ε is the dissipation constant and length scale [10].

The TKE model in Veros allows for different values of the three parameters, c_k, c_ε and α_{tke}, but also minimum values for vertical viscosity and diffusivity, κ_m and κ_h. The default values for the three parameters are $c_k = 0.1$, $c_\varepsilon = 0.7$ and $\alpha_{tke} = 30$ and the Prandtl number, P_{rt}, is set to 10 by default. The minimum values for κ_m and κ_h, and c_k and c_ε will be tuned in this project.

3.3.2 Horizontal mixing

Horizontal viscosity is given by the constant value A_h and is scaled with $\cos(\varphi)^n$, where φ is the latitude and n is a cos power that can be chosen in Veros [14]. This scaling is used as the grid spacing decreases towards the poles, requiring a corresponding reduction in viscosity [11]. A_h will be tuned in this project.

3.3.3 Isoneutral mixing

It is established that tracer mixing along isoneutral directions dominates over dianeutral mixing. Here, the isoneutral direction refers to the direction along the tangent to the potential density

surface [12]. Veros offers an isoneutral mixing scheme following the formulation by Griffies (1998), where horizontal diffusion is parameterized as diffusion along the isoneutral directions. This scheme becomes numerical unstable in regions with a too steep slope, so to preserve the stability a scaling, d_{taper}, is introduced:

$$d_{taper} = \frac{1}{2}\left(1 + \tanh\frac{s_c - |s|}{s_d}\right) \tag{14}$$

with s being the slope of the isoneutral surface and s_c and s_d parameters that can be set as variables in Veros. s_c is the critical slope. The isoneutral diffusivity used in this scheme is then given by $K_{iso,0}$ multiplied by the scalar, d_{taper}, in regions with slopes smaller than the critical slope, and by $K_{iso,steep}(1-d_{taper})$ in regions with slopes steeper than the critical slope [8]. $K_{iso,0}$ and $K_{iso,steep}$ are parameters that can be chosen in Veros and they will be tuned in this project.

3.4 Small scale coastal ocean modelling

Veros has yet to be configured for smaller model domains and even though it is the same governing equations that are solved no matter the scale, there are still differences between large scale ocean modelling and small scale coastal modelling. The limited spatial extent of a fjord demands a much higher horizontal resolution than used in global ocean modelling, and the shallow depth and complex bathymetry demand higher vertical resolution throughout the whole water column, whereas global ocean models can exploit the deep waters and use lower resolution toward the bottom. Due to a shallower depth and the smaller spatial extent, fjords will react stronger and on smaller time scales on external forcing, than the global ocean.

As fjords are connected to the coastal water, the model has a boundary at the interface between the model domain and the coastal water. Open boundaries are in some coastal ocean models forced with data from a coarser resolution model run in an one-way or a two-way approach [17]. Veros does not yet support the implementation of open boundary conditions, instead, a salinity sponge layer has been implemented at the interface, which is further described in the forcing section later in this thesis. A consequence of this is, among other things, reflection at the interface.

Furthermore, variations in surface elevation due to tides and storms are, relative to average depth, higher in fjords than in global oceans and can therefore add to the dynamics [17]. Veros uses a rigid lid approximation and does not support a free surface formulation, so variations in the surface elevation are not included in the model. Given that the main focus in this project is the estuarine and intermediary circulation, both of which are tidally averaged, and considering that the Gullmar fjord is characterized by weak tides, it is deemed acceptable to keep the rigid lid approximation.

4 Methods

The approach in this project has been to initially set up a model of the Gullmar fjord with minimized noise, by changing the parameters used in Veros, followed by the introduction of various forcing to investigate the resulting circulation. The number of possible runs during the

project has been limited by the high computational time; the model needs to run approximately 3 hours on the Aegir HPC per model day output.

In the following sections the setup of the model domain, the definition of noise, and an overview of the changed parameters and the different forcing are presented.

4.1 Model domain

Bathymetry data for the Gullmar fjord was provided by Göran Broström (Göteborgs University) via personal communication. The bathymetry is rotated 50 degrees to minimize the model domain area necessary to cover the whole fjord, and all model results in this thesis are therefore shown in the rotated coordinate system. The model domain is discretized with 160 $\times$ 380 horizontal grid points, which makes a horizontal resolution of approximately 93 m $\times$ 97 m in the zonal and meridional directions. In the vertical direction, the grid consists of 23 equally spaced layers, with a resolution of 5 m, so the model uses geopotential vertical coordinates, which means that the vertical coordinates are independent of time and location [17]. The time step used in the model is $\Delta t = 3s$. Figure 3 shows the Gullmar fjord and its bathymetry. This figure is made using the model output from Veros and it is therefore possible to see, how high the horizontal resolution is.

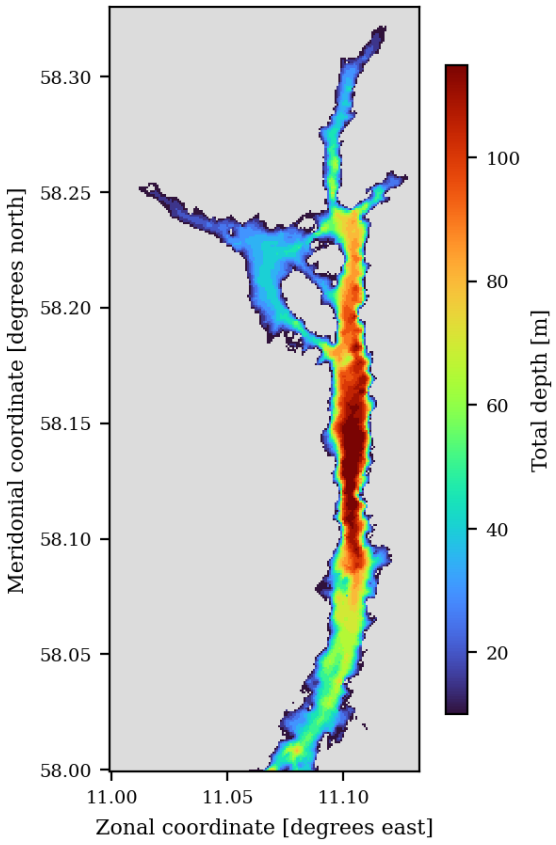

Figure 3: Figure of the bathymetry of the Gullmar fjord, made using the model output from Veros. Note that the coordinates used here is the rotated coordinates.

4.2 Noise

Numerical instabilities on the grid scale, called noise, are created through the various numerical schemes used to solve the primitive equations and are unwanted, as it lead to numerical mixing. A great amount of the grid scale noise is created as the flow moves over steep bathymetry [16] and especially rigid lid streamfunction models, which Veros is, are prone to grid scale noise in regions with steep bathymetry [11]. The geopotential vertical layers used in Veros will lead to a step-wise discretization of the bathymetry, which may increase the noise at the boundary even more. Increased viscosity decrease grid scale noise, but at the expense of a less precise model solution [16]. It is therefore necessary to find a compromise between a lower viscosity which results in a better model solution, but more noise, and a higher viscosity which results in less noise, but also in a less precise model solution.

In this project, the noise will be quantified by the variation of the velocity between grids, as the absolute difference between the velocity and the smoothed velocity, as done in Jochum

(2008)[16]. So the noise at one point is defined as:

$$noise = \frac{1}{3}\sum_{i=1}^{3} |u_i - u_{i,smooth}| \tag{15}$$

where the sum sums over the velocities in the x-, y- and z-directions. The velocity in the x-direction, u, are smoothed in the x-direction, v in the y-direction, and w in the z-direction, all with a three point triangular filter with weights 0.25, 0.5, 0.25. Thus, the smoothed u velocity are defined as:

$$u^{i,j,k}_{smooth} = \frac{u^{i-1,j,k} + 2u^{i,j,k} + u^{i+1,j,k}}{4} \tag{16}$$

and similar for v and w. At boundaries, the velocities are smoothed with a two point filter with weights 0.75, 0.25. To better compare the noise between the different setups, the noise is normalized using the min-max feature scaling.

4.3 Changing the parameters

To optimize the model, different values for the parameters outlined in the ocean modelling section will be tested. Given the extensive computational time required to run the model, testing a large number of parameters is not possible. However, the primary focus has been to investigate how variations of these parameters may influence the noise and model solution. Determining the exact optimal parameter values lies beyond the scope of this project. The different parameters that have been tuned in this project are presented in table 1.

Parameter	Description	Original value
`A_h`	Lateral viscosity	$1.0\frac{m^2}{s}$
`kappaM_min`	Minimum viscosity	$2 \cdot 10^{-4}\frac{m^2}{s}$
`kappaH_min`	Minimum diffusivity	$2 \cdot 10^{-5}\frac{m^2}{s}$
`c_k`	c_k value used in the TKE scheme	0.1
`c_eps`	c_ε value used in the TKE scheme	0.7
`K_iso_0`	Isoneutral diffusivity	$1.0\frac{m^2}{s}$
`K_iso_steep`	Used in regions with steep slopes	$1.0\frac{m^2}{s}$
`enable_noslip_lateral`	Used to enable noslip boundary condition	`False`

Table 1: Parameters used in this project with descriptions and original values. The original values refer to the parameter values used in the original setup of the fjord. Later in this thesis, the original setup is called setup 1.

4.4 The spin-up period

When the model is initialized, the water in the fjord is at rest and the salinity and temperature profiles are determined by chosen initial conditions. The model is thus not in a physically realistic state yet, so before model data can be collected, the model should run until it converges to a steady state, this is called the spin-up period. The spin-up time may vary for different setups and in order to check if the model has reached the spin up time, state variables from the spin-up period are collected and plotted as a function of model time.

For each new combination of parameters, the model must be reinitialized and undergo the spin-up period again. This is necessary to prevent any noise generated during previous simulations from propagating into the new setup. However, once a model setup with a set of parameters has completed the spin-up period, different forcings can be introduced, and the model must undergo another, but much shorter, spin-up period, as the model is already in a physically realistic state after the initial spin-up period.

4.5 Forcing

Veros provides the opportunity to add a variety of different forcing. Since the aim of this study is to examine whether estuarine and intermediary circulation can be established in the model fjord, it is relevant to apply forcing through freshwater input and density variations of the coastal water. As this study does not focus on the seasonal impact on the circulation, the model will not be forced by temperature changes.

Veros do not provide the opportunity to use open boundaries or add a freshwater source, but instead use restoring boundary conditions, explained below, at the surface and at the head of the mouth, where the fjord connects to the coastal water.

4.5.1 Freshwater supply by restoring salinity surface forcing

As Veros uses the rigid lid approximation, the effect of the freshwater supply must be parameterized by introducing a virtual salt flux, that removes salt. The surface salt flux is calculated as a restoring term, that forces the surface salinity to go towards a prescribed surface salinity field:

$$F_V = \frac{dS}{dt} = \frac{1}{t_{res}}(S_{ref} - S) \tag{17}$$

with S_{ref} being the prescribed salinity field, t_{res} the restoring time and S the actual surface salinity. The equivalent freshwater flux, F_W, can then be determined as [23]:

$$F_W = -\frac{F_V}{S} \tag{18}$$

To obtain the total value of the freshwater supply to the fjord, which is used to calculate the estuarine circulation in equation (4), the freshwater flux, F_W, can be integrated over the entire fjord. To better simulate a greater freshwater supply towards the fjord's head, where there is more land freshwater runoff and river discharge, the prescribed salinity field in the model used in this thesis has been defined as a linear function, with a higher salinity towards the mouth and a lower salinity towards the head.

4.5.2 Salinity sponge layer

The salinity sponge layer is used as a restoring boundary condition for the salinity at the mouth of the fjord. The restoring term is calculated in the same way as in equation (17). The prescribed salinity field, S_{ref}, can either be constant in time or be time dependent. If S_{ref} is constant in time, there will be no variations of the density in the coastal water and consequently no forcing of the intermediary circulation. Knudsen's relations will initially be examined without forcing the intermediary circulation and then it will be attempted to introduce a time-dependent salinity

sponge layer forcing. The salinity sponge layer region in this model is the layer containing the two meridional grid points closest to the mouth.

4.5.3 Surface wind stress

The surface wind stress forcing applied in the model during this project is idealized. Due to the elevated coastlines around Gullmar fjord, it is assumed that the surface wind is in the along fjord direction at all times, so the surface wind stress in the x-direction is set to zero: $\tau_x = 0$. Note that the x-direction here refers to the rotated coordinates so that the x-direction is the across fjord direction. It is furthermore assumed that the wind stress is spatially uniform. The wind stress amplitude is calculated as:

$$\tau_y = C_d \rho_{air} w^2 \tag{19}$$

where $C_d = 0.0011$ is a drag coefficient, $\rho_{air} = 1.2 kg/m^3$ is the density of air and w is the wind speed [2]. The wind speed is estimated by looking at the wind velocity data from Kristineberg, which is located at the mouth of the Gullmar fjord, presented in Arneborg (2004) [4].

4.5.4 Overview of the different forcing cases

Five different forcing cases will be tested in this project. A brief explanation of the five cases is now presented, for more detailed information about the cases see appendix A.

The same salinity surface forcing is applied to all five cases. The salinity sponge layer is time independent for case 1, 2, and 3 and there is thus no forcing of the intermediary circulation in these cases. Case 1 is without wind, in case 2 an oscillating wind stress in the along fjord direction is added with a period of 2 days and an amplitude on $0.05 \frac{N}{m^2}$, and in case 3 a constant wind stress going into the fjord with an amplitude of $0.132 \frac{N}{m^2}$ is added. The salinity sponge layer is time dependent in case 4 and 5; in case 4 it is set to vary between two different salinity profiles with a period of 20 days to force the intermediary circulation, and in case 5 it is attempted to model deep water renewal by increasing the salinity in the sponge layer.

5 Results and discussion

5.1 Setting up the model

To set up the model, the noise is minimized by changing the parameters presented in table 1. To illustrate the tuning process with the different tested values for the parameters and the corresponding selected values, a diagram of the process and the decisions made along the way is presented in Figure 4. Each model setup has completed the spin-up period, which took about 50 model days (approximately seven days of computation time) before the model solution was analyzed. The best values are determined based on the noise levels, but also through an analysis of the salt distribution and the circulation within the fjord, to ensure that the values result in a realistic fjord model. An overview of the resulting noise levels in the setups can be seen in table 2.

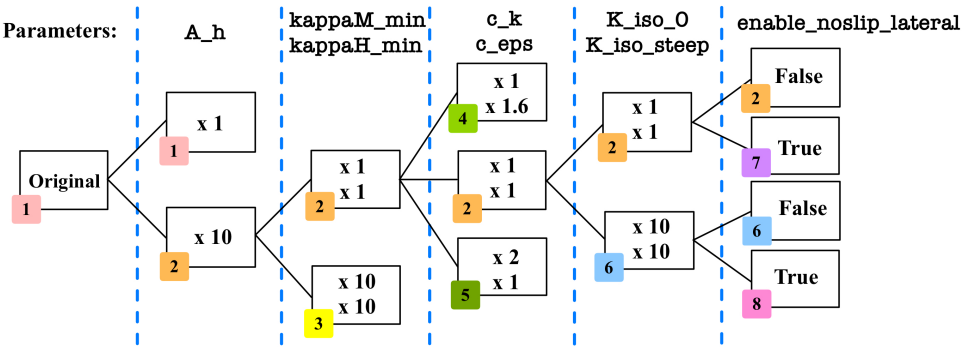

Figure 4: Illustration of the tuning process. The colored numbers show which setup each box represents and the factors in the boxes are the value of the respective parameter (written at the top) relative to the original setup (setup 1). For example: in setup 5, c_k is two times higher than the original value, c_ε is the same as the original value, $\kappa_{M,min}$ and $\kappa_{H,min}$ is the same as the original and A_h is ten times higher than the original value.

Setup	1	2	3	4	5	6	7	8
Noise $[\cdot 10^{-2}]$	2.71	1.41	0.68	1.36	1.49	1.18	1.26	1.16

Table 2: Normalized noise determined with equation (15) averaged over the whole fjord for the eight setups. Note that the noise is dimensionless as it is normalized.

As seen in Figure 4, the first parameter that has been varied is the horizontal viscosity, A_h. Two different values were tested and it was found that an increase in A_h significantly reduces the noise, see setup 1 and 2 in table 2.

The model solution from setup 2 shows a circulation of an upper outgoing layer and a lower ingoing layer, see Figure 5(a), where the zonally averaged along fjord velocities are plotted, this is considered to align with the described theory. The upper layer reaches down to a depth of 5 m and the lower layer lies between 5 m and 15 m depth. These layers are thus not very deep, so in setup 3 it is explored if an increase in the values for the minimum vertical diffusivity and viscosity results in deeper layers. The zonally averaged along fjord velocities from setup 3 is plotted in Figure 5(b), where it is observed that an increase in the two minimal vertical mixing values does indeed result in deeper ingoing and outgoing layers in the fjord. Furthermore, as seen in table 2, setup 3 has a significantly lower noise level than setup 2. But the increased minimum vertical mixing values also result in the fjord becoming highly mixed, thereby reducing the salinity difference between the surface water and the bottom over time, shown in Figure 5(c). It is not realistic that the salinity of the bottom water increases over time and it is therefore determined that the original values for the minimum vertical viscosity and diffusivity are the best choice and these values are used in the following setups, even though the increased values minimized the noise.

Setup 4 and 5 test the model with increased dissipation constant, c_ε, and mixing coefficient, c_k. Setup 4 slightly reduced the noise compared to setup 2 and setup 5 resulted in increased noise. Nevertheless, the following setups were run without increasing c_ε. Due to the high computational time and the small difference in noise between setup 2 and 4, it has been determined that re-running them with the increased c_ε value is not worthwhile.

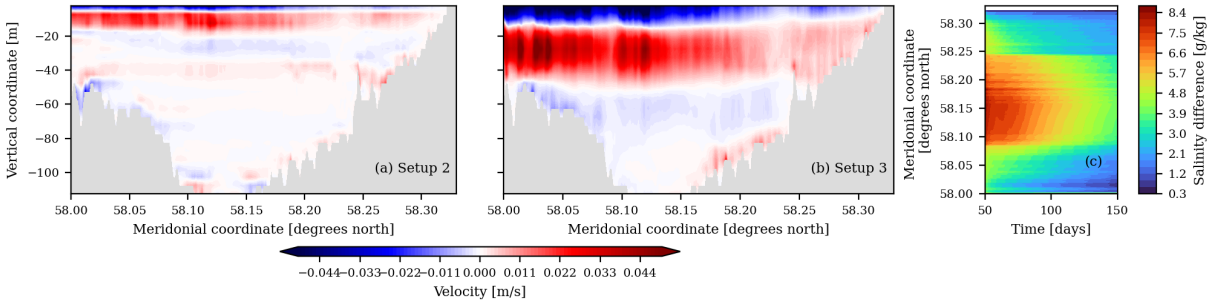

Figure 5: Zonally averaged along fjord velocities for (a): setup 2, (b): setup 3. (c): Zonally averaged salinity difference between the bottom and the top of the fjord as a function of time for setup 3.

In setup 6 the isoneutral mixing is increased by increasing $K_{iso,0}$ and $K_{iso,steep}$. This reduces the noise by approximately 16% compared to setup 2, see table 2, while the circulation and salinity distribution don't change significantly, see appendix C.

In setup 7, it is explored which impact no-slip lateral boundary conditions have on the noise, so it is tested with the original isoneutral mixing values, see Figure 4. The resulting noise in setup 7 is reduced by approximately 11% compared to setup 2, see table 2. When looking at the model circulation from setup 7, see appendix C, it can be seen that, compared to the circulation in setup 2, the lower layer deepens. This is considered realistic.

In setup 8 both the increased isoneutral mixing and the no-slip lateral boundary conditions are used. As seen in table 2, this reduces the noise by approximately 18% compared to setup 2.

Based on the determined noise and an analysis of the model solutions, it is concluded that setup 8 has the best parameter values. Setup 3 resulted in a significantly lower noise level, but don't result in a realistic fjord model.

5.1.1 Spatial distribution of the noise

Figure 6 shows a spatial distribution of the noise in the fjord for setup 2 and 8, where the zonally and horizontally averaged noise is plotted for both setups. This makes it possible to investigate where the noise is highest and where it is minimized through changes in the parameters.

When looking at the zonally averaged noise, it is generally observed that the noise is highest along bathymetry, especially near steep bathymetry, which was expected. Much of the noise is also generated in the upper layers of the fjord, where the circulation takes place. By plotting the depth averaged noise for the upper 22.5 m, shown in appendix D, it is seen that the largest part of the noise in the upper layers is created along the bathymetry as well. The area around 40 m depth near 58.20 degrees north also has higher noise levels. By plotting the depth averaged noise between depths of 37.5 m and 47.5 m, see appendix D, it is seen that this noise primarily is created along the bathymetry in the water west for the island Bornö.

In Figure 6 it is observed that the increase in isoneutral mixing and the no-slip boundary condition, setup 8, mostly reduces the noise between depths of 30 m and 60 m, and below 80 m, compared to setup 2. When looking at the zonally averaged noise, it is clear that the noise

reduction is dominant along the bathymetry, especially near steep bathymetry, for example close to the mouth or at 58.25 degrees north.

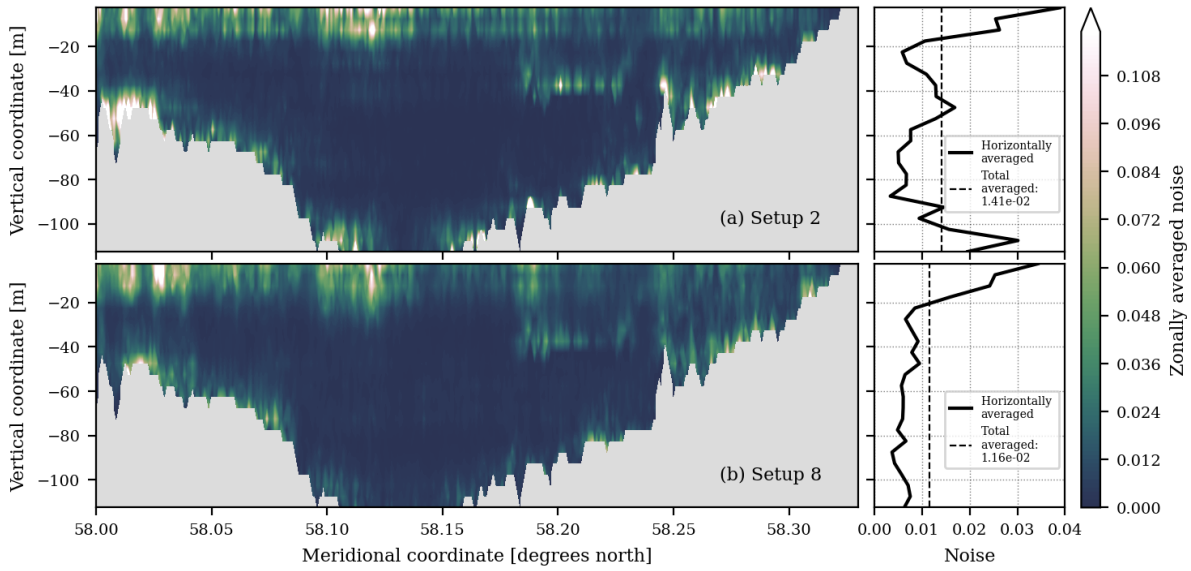

Figure 6: Comparison of the noise for (a): setup 2, (b): setup 8. To the left: Zonally averaged noise. To the right: full lines are depth profiles of the noise (so horizontally averaged noise) and the dashed lines are the totally averaged noise. Note that as the noise is normalized it's dimensionless.

5.2 Analyzing the circulation

The parameters from setup 8 are now used in a model setup of the fjord, where the various forcing cases described in section 4.5.4 will be tested and the resulting circulation will be determined and compared with the presented theory on fjords.

5.2.1 Case 1: linear surface salinity forcing

In Figure 7(a), the zonally averaged along fjord velocity and salinity are shown for case 1. It is seen, that the salinity is greater towards the head and that the forcing results in a circulation of an upper outgoing layer and a deeper ingoing layer underneath. The basin water is almost completely stagnant. This circulation is thus consistent with the described theory of estuarine circulation. The Knudsen transport and the model integrated transport in the two layers are compared in Figure 8(a). The surface salinity forcing in this case results in a total freshwater flux that is determined to be $F_W = 23.4m^3s^{-1}$, which is approximately the same flux as the river discharge into the head in the Gullmar fjord. When comparing the Knudsen and model transports, it is observed that Knudsen's relations determine the transport well in the middle of the fjord, roughly between 58.08 and 58.22 degrees north, but overestimate the transport in the rest of the fjord. As explained earlier, Knudsen's relations are best applied in regions with no turbulent mixing and with strong vertical stratification. Because of the closed boundary conditions used at the mouth in the model setup, reflections can occur at the interface, which can result in more mixing and the salinity difference between the two layers thus decreases and the Knudsen transport increases. This may be an explanation for the high Knudsen transport

toward the mouth. Furthermore, the closed boundary condition at the mouth also results in a velocity of zero and the model transport thus goes towards zero at the mouth, which is not realistic. This results in an even higher difference between the Knudsen and model integrated transports at the mouth.

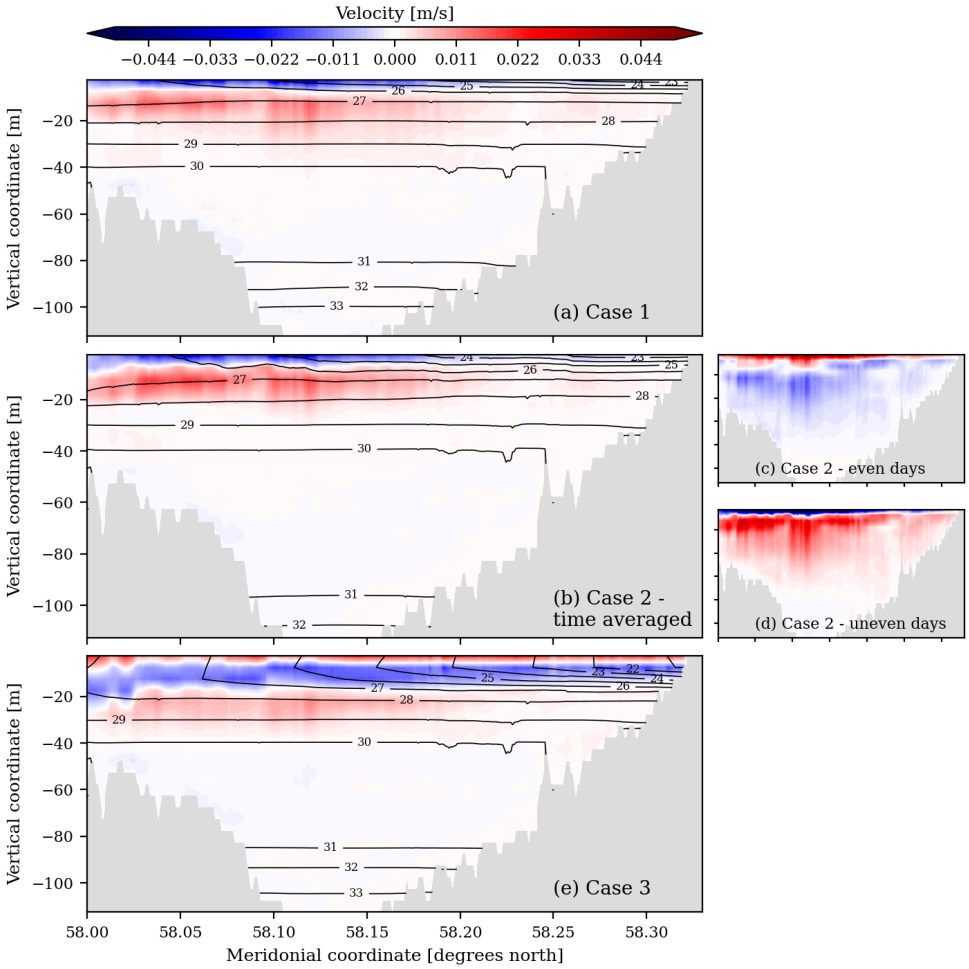

Figure 7: Zonally averaged along fjord velocities (m/s) and salinity contours (g/kg) for: (a): case 1, (b): case 2 averaged over 10 days, (c): even days in case 2, (d): uneven days in case 2, (e): case 3. Note that negative velocities are directed out of the fjord and positive into the fjord.

5.2.2 Case 2: added oscillating wind

In case 2, the case of added oscillating surface wind stress, a resulting wind driven circulation is forced, this is shown in Figure 7(c) and (d), where the zonally averaged along fjord velocity are plotted for an even day and an uneven day. It can be observed that the wind stress is strong enough to inverse the direction of the two layers so that the upper layer flows in the same direction as the wind and the lower layer flows in the opposite direction. The circulation is thus changing direction every day, just as the wind. To test if Knudsen's relations still hold for this case, the data is averaged over 10 days, and it is then investigated if Knudsen's relations can estimate the time averaged transport. The zonally averaged along fjord velocity and salinity contours averaged over 10 days are shown in Figure 7(b) and it is clearly observed that the time averaged circulation resembles the circulation in case 2 seen in Figure 7(a); there is an upper

outgoing layer and a lower ingoing layer. The salinity contours for the two cases also mostly resemble each other, but when looking at the basin water in case 2 it can be seen that it is less salty than in case 1. This could be attributed to the added oscillating wind, which may increase the mixing, leading to a reduction in the salinity of the basin water. That the time averaged circulation in case 2 resembles the circulation in case 1 can also be seen when comparing the Knudsen transport and the model integrated transport for the time averaged data, see Figure 8(b). Knudsen's relations can approximately determine the transport in the middle of the fjord, but overestimate the transport, especially towards the mouth of the fjord. The model transport in case 1 and the time averaged model transport in case 2 are approximately the same throughout the fjord. The circulation in case 2 is therefore in a superposition of a time dependent wind driven circulation and a constant estuarine circulation and when averaging over time, only the estuarine circulation is apparent.

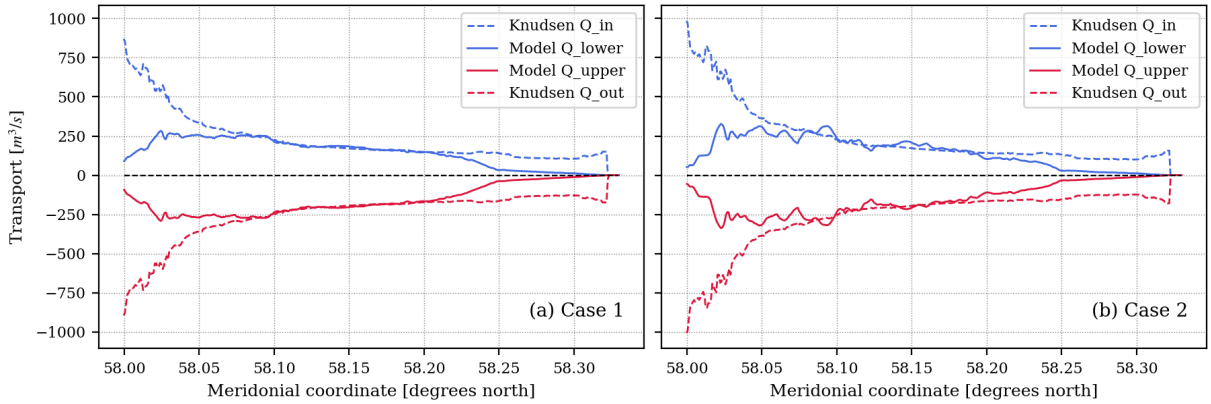

Figure 8: Comparison between the transport, Q, in the two layers determined by integrating the model solution along fjord velocity (solid lines) and calculated with Knudsen's relations (dashed lines). (a): for the circulation in case 1, (b): for the 10 day averaged circulation in case 2.

5.2.3 Case 3: added constant wind

Just like in the case of added oscillating wind, the added constant wind in case 3 results in a wind driven flow. This flow is stronger than the estuarine circulation and because the wind stress is going inwards at all times, the resulting circulation is an inverse circulation with an upper ingoing layer and a lower outgoing layer, see Figure 7(e). When looking at the zonally averaged salinity distribution in the fjord in this case, Figure 7(e), it is observed that the inverse circulation causes downwelling at the head and the fresher water is therefore transported down and outwards with the middle outgoing layer. Because the circulation is inverse, Knudsen's relations can't be used in this case. Again, it is supposed that the circulation must be in a superposition of the wind-driven and estuarine circulation. It may be possible to determine the wind-driven circulation and subtract it from the total flow and then test Knudsen's relations on the resulting circulation, but this is not done in this project. In (Arneborg and Liljebladh, 2009) they describe a period with smaller variations of the coastal water stratification and thus weaker forcing of the intermediary circulation. It is described that the current therefore has a general estuarine circulation pattern, but that this circulation is broken by strong wind that pushes water into the fjord and creates an inverse exchange [3]. So it is observed that a strong ingoing

wind breaks the estuarine circulation and creates inverse exchange in the Gullmar fjord. The resulting measured along fjord velocities under this period have an amplitude of about $0.25m/s$ at the mouth and about $0.15m/s$ inside the fjord [3]. When comparing these velocities with the model solution velocities seen in Figure 7(e) it is seen, that these are between $0.1m/s$ and $0.2m/s$ slower than measured and presented in the (Arneborg and Liljebladh, 2009) paper.

5.2.4 Case 4: variations in sponge layer salinity forcing

By making the sponge layer salinity forcing vary in time, the intermediary circulation is forced. Figure 9(a) shows the along fjord velocity and the isohalines in the middle of the fjord at approximately 3900 m from the mouth (see appendix E for exact location) as a function of time. It is clearly observed that the variation of density in the coastal water forces a circulation dependent on time and that this circulation is stronger than the estuarine. When the isohalines rise, the upper layer flows outwards and the lower layers flow inwards and as the isohalines descends, the upper layer flows inwards and the lower layer outwards. This is in agreement with the described theory of intermediary circulation.

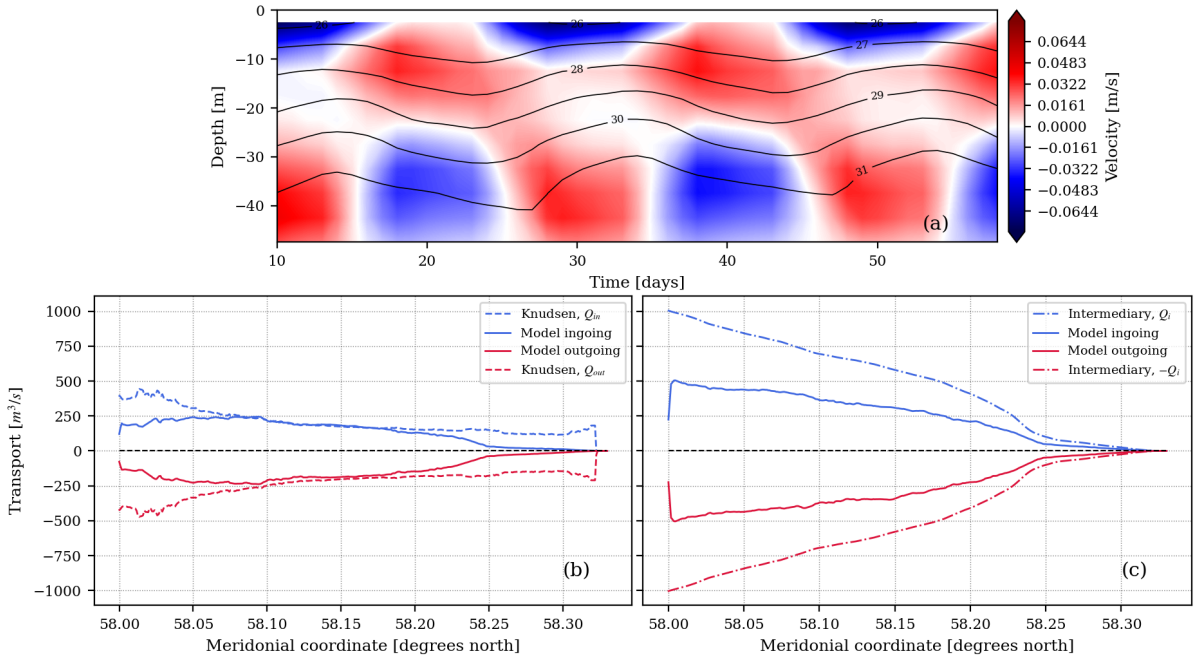

Figure 9: (a): Salinity contours in units g/kg and along fjord velocity in the middle of the fjord about 3900 m from the mouth as a function of time for case 4. (b): comparison between model transport in the two upper layers and the transport estimated with Knudsen's relations for model outputs averaged over 20 days. (c): comparison between ingoing and outgoing model transport averaged over 20 days and the transport estimated with the empirical formula for intermediary circulation, Q_i. For both (a), (b) and (c), positive velocity or transport are directed into the fjord and negative values out of the fjord.

The circulation in case 4 is in a superposition of a steady estuarine circulation and a time dependent intermediary circulation. Because the forcing of the intermediary circulation is periodic, it must be possible to determine the steady estuarine circulation by time averaging over a period. The result is seen in Figure 9(b), where it is clear the background circulation is the estuarine

circulation and that it resembles the estuarine circulation seen in case 1 and 2, which makes sense as the same surface salinity forcing is applied.

If, instead, ingoing and outgoing transport is determined for each day and then time averaged over the period, the magnitude of the intermediary circulation can be explored. The average ingoing and outgoing model transport is compared with the empirical formula for the intermediary circulation, $Q_i(y)$ from equation (5) and (7), in Figure 9(c). Q_i is larger than the model transport throughout the fjord. As previously mentioned, equation (5) is an empirical formula that does not include damping of the intermediary circulation with increasing distance to the mouth, which is observed in the Gullmar fjord. This may thus contribute to an overestimated transport. It can also be seen in the figure that the model solution transport again goes towards zero at the mouth because of the closed boundary conditions, which may contribute to a smaller model transport.

The zonally averaged along fjord velocity for each day for case 4 is shown in appendix F. It is observed that with increasing time, there is an increase in both movement and noise within the basin water, which isn't realistic.

Case 4 demonstrates that it is possible to force intermediary circulation by varying the density at the mouth through the salinity sponge layer and that it is possible to estimate the steady estuarine circulation with Knudsen's relations.

5.2.5 Case 5: can basin water renewal be modeled?

As described in the theory section, the basin water is mainly stagnant and is only renewed when the salinity of the coastal water above the level of the sill exceeds the density of the basin water. By increasing the salinity in the sponge layer over time, it is explored if basin water renewal can

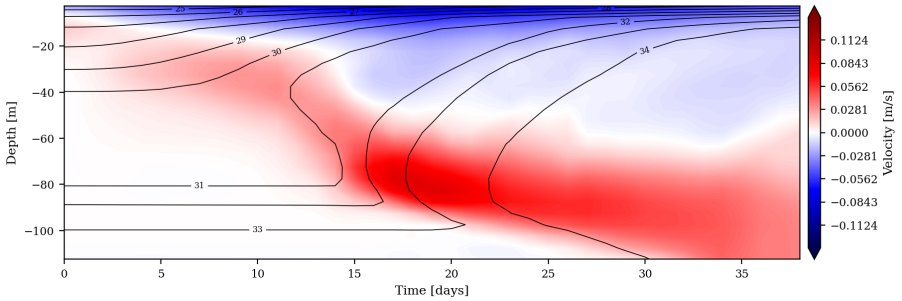

Figure 10: Salinity contours in unit g/kg and along fjord velocity as a function of time for case 5 at one of the deepest parts in the fjord.

be modeled. Figure 10 shows the along fjord velocity and salinity at one of the deepest parts of the fjord as a function of time (see appendix G for exact location). In the first few days, the estuarine circulation is dominating, but as the salinity increases, it is seen that the ingoing and outgoing layers deepen and reach the basin water. The higher salinity at the mouth thus gives rise to basin water renewal, just as the theory describes. The velocity of the two layers has a higher amplitude than seen in the other cases. In the review paper about fjords by Inall and Gillibrand (2010) they present typical maximum current speeds for various types of circulation. The maximum current speed of the estuarine and intermediary circulation is in the range of

0.01-0.2 m/s, but the renewal of the basin water is in the range of 0.1-0.4 m/s [15]. So, the higher velocities during basin water renewal are realistic.

6 Outlook and conclusion

In this project, Veros has been used to set up a model of the Gullmar fjord and it is demonstrated that the estuarine, intermediary, and wind-driven circulations, as well as basin water renewal, can be forced and successfully compared with existing theory on fjords.

Various parameters used in the numerical scheme in Veros were tested to minimize the noise in the model and it was found that increased horizontal viscosity, increased isoneutral mixing and no-slip boundary condition resulted in the least noise and a realistic model solution. To further minimize the noise, it would be relevant to smooth out the bathymetry, as much of the noise was generated along the boundaries.

Veros does not yet support open boundaries and that is apparent in the model results from the fjord; the closed boundary at the mouth resulted in reflections and velocities going towards zero at the mouth. The model can thus be improved by implementing open boundaries at the interface between fjord and coastal waters.

Five different cases were tested in the model. The initial conditions and applied forcing for all cases were highly idealized and did not represent the true conditions in the Gullmar fjord. Therefore, it has not been possible to compare the model results directly with observations from the Gullmar fjord. Instead, the model results were compared with existing theory about circulation in fjords. It can be concluded that it is possible to force both an estuarine, a wind-driven, and an intermediary circulation. Knudsen's relations were used to estimate the transport due to the estuarine circulation and the relations estimated the transport well in the middle of the fjord, away from the mouth and the head, both in the case of no wind, in the case of added oscillating wind and in the case of forced intermediary circulation. An empirical formula for intermediary exchange was compared with the model transport in the case of forced intermediary circulation and it was seen, that the formula resulted in larger transport than the model transport throughout the whole fjord. By increasing the salinity, and thus the density, at the mouth, renewal of the basin water has been modeled.

For future work, it would be interesting to initialize the model with a more realistic salinity profile and force it with observed wind and observed density variations of the coastal water. This will allow for a direct comparison between the model solution and observational data from the Gullmar fjord.

7 Acknowledgment

Thanks to Markus Jochum for being my supervisor and for introducing me to the complexity of the ocean. Thanks to Roman Nuterman for implementing the bathymetry of the Gullmar fjord in Veros and for your guidance on how to use the Aegir cluster. Thanks to Marta, Qifan, Asger, and Jeppe for your support and good times at the office and at Bornö.

References

[1] Lars Arneborg. "Turnover times for the water above sill level in Gullmar Fjord". In: *Continental Shelf Research* 24.4-5 (Mar. 2004), pp. 443–460. ISSN: 02784343. DOI: 10.1016/j.csr.2003.12.005.

[2] Lars ARNEBORG and Bengt LILJEBLADH. "The internal seiches in Gullmar Fjord. Part I : Dynamics". eng. In: *Journal of physical oceanography* 31.9 (2001), pp. 2549–2566. ISSN: 0022-3670. DOI: 10.1175/1520-0485(2001)031<2549:TISIGF>2.0.CO;2.

[3] Lars Arneborg and Bengt Liljebladh. "Overturning and dissipation caused by baroclinic tidal flow near the sill of a fjord basin". In: *Journal of Physical Oceanography* 39.9 (Sept. 2009), pp. 2156–2174. ISSN: 00223670. DOI: 10.1175/2009JPO4037.1.

[4] Lars Arneborg et al. "Spatial variability of diapycnal mixing and turbulent dissipation rates in a stagnant fjord basin". In: *Journal of Physical Oceanography* 34.7 (July 2004), pp. 1679–1691. ISSN: 00223670. DOI: 10.1175/1520-0485(2004)034<1679:SVODMA>2.0.CO;2.

[5] Thomas S. Bianchi et al. *Fjords as Aquatic Critical Zones (ACZs)*. Apr. 2020. DOI: 10.1016/j.earscirev.2020.103145.

[6] Hans Burchard et al. *The Knudsen theorem and the Total Exchange Flow analysis framework applied to the Baltic Sea*. July 2018. DOI: 10.1016/j.pocean.2018.04.004.

[7] E. D. Cokelet and R. J. Stewart. "The exchange of water in fjords: the efflux/reflux theory of advective reaches separated by mixing zones." In: *Journal of Geophysical Research* 90.C4 (1985), pp. 7287–7306. ISSN: 01480227. DOI: 10.1029/JC090iC04p07287.

[8] Carsten Eden. *pyOM2.0 documentation*. Tech. rep. 2014.

[9] David M Farmer and Howard J Freeland. *The Physical Oceanography of Fjords*. Tech. rep. 1983, pp. 147–220.

[10] Philippe Gaspar, Yves Grégoris, and Jean-Michel Lefevre. "A simple eddy kinetic energy model for simulations of the oceanic vertical mixing: Tests at station Papa and long-term upper ocean study site". In: *Journal of Geophysical Research: Oceans* 95.C9 (Sept. 1990), pp. 16179–16193. ISSN: 0148-0227. DOI: 10.1029/jc095ic09p16179.

[11] Stephen M Gries et al. *Developments in ocean climate modelling*. Tech. rep. URL: http://www.ifremer.fr/lpo/WGOMD/.

[12] Stephen M Griffies et al. *Isoneutral Diffusion in a z-Coordinate Ocean Model*. Tech. rep. 1998.

[13] Dion Häfner, Roman Nuterman, and Markus Jochum. "Fast, Cheap, and Turbulent—Global Ocean Modeling With GPU Acceleration in Python". In: *Journal of Advances in Modeling Earth Systems* 13.12 (Dec. 2021). ISSN: 19422466. DOI: 10.1029/2021MS002717.

[14] Dion Häfner et al. "Veros v0.1 - A fast and versatile ocean simulator in pure Python". In: *Geoscientific Model Development* 11.8 (Aug. 2018), pp. 3299–3312. ISSN: 19919603. DOI: 10.5194/gmd-11-3299-2018.

[15] M. E. Inall and P. A. Gillibrand. "The physics of mid-latitude fjords: a review". In: *Geological Society, London, Special Publications* 344.1 (Jan. 2010), pp. 17–33. ISSN: 0305-8719. DOI: 10.1144/SP344.3. URL: https://www.lyellcollection.org/doi/10.1144/SP344.3.

[16] Markus Jochum et al. “Ocean viscosity and climate”. In: *Journal of Geophysical Research: Oceans* 113.6 (June 2008). ISSN: 21699291. DOI: 10.1029/2007JC004515.

[17] Knut Klingbeil et al. *The numerics of hydrostatic structured-grid coastal ocean models: State of the art and future perspectives*. May 2018. DOI: 10.1016/j.ocemod.2018.01.007.

[18] Pijush K. Kundu, Ira M. Cohen, and David R. Dowling. *Fluid Mechanics*. 6th. Elsevier, 2016. ISBN: 9780124059351. DOI: 10.1016/C2012-0-00611-4.

[19] C. Smeaton and W. E.N. Austin. “Understanding the Role of Terrestrial and Marine Carbon in the Mid-Latitude Fjords of Scotland”. In: *Global Biogeochemical Cycles* 36.11 (Nov. 2022). ISSN: 19449224. DOI: 10.1029/2022GB007434.

[20] Anders Stigebrandt. “Hydrodynamics and Circulation of Fjords”. eng. In: *Encyclopedia of Lakes and Reservoirs*. Encyclopedia of Earth Sciences Series. Dordrecht: Springer Netherlands, 2012, pp. 327–344. ISBN: 1402056168. DOI: 10.1007/978-1-4020-4410-6{_}247.

[21] Artur Svansson. *Bornö Hydrographie Station with R/V Skagerak (I) MEDDELANDE FRÅN HYDROGRAPHY OF THE GULLMAR FJORD (GULLMARSFJORDENS HYDROGRAFI)*. Tech. rep. 1984.

[22] Geoffrey Vallis. *Atmospheric and Oceanic Fluid Dynamics*. 4th ed. Cambridge University Press, 2017, pp. 0–946.

[23] Jianjun Yin et al. “Evaluating the uncertainty induced by the virtual salt flux assumption in climate simulations and future projections”. In: *Journal of Climate* 23.1 (Jan. 2010), pp. 80–96. ISSN: 08948755. DOI: 10.1175/2009JCLI3084.1.

Appendices

A Case forcings

For all 5 cases

Initial salinity profile: `np.linspace(34, 26, settings.nz)`

Surface salinity forcing: `np.linspace(30, 16, settings.ny + 4)`

Surface forcing restoring time: 10 days

For case 1

Meridional wind stress: $\tau_y = 0$

Salinity sponge layer forcing: `np.linspace(34, 30, settings.nz)`

Sponge layer forcing restoring time: 10 days

For case 2

Meridional wind stress: $\tau_y(t) = 5 \cdot 10^{-2} \cos \frac{2\pi t}{2 \cdot 86400s}$

Salinity sponge layer forcing: `np.linspace(34, 30, settings.nz)`

Sponge layer forcing restoring time: 10 days

For case 3

Meridional wind stress: $\tau_y = 0.132 \frac{N}{m^2}$

Salinity sponge layer forcing: `np.linspace(34, 30, settings.nz)`

Sponge layer forcing restoring time: 10 days

For case 4

Meridional wind stress: $\tau_y = 0$

Salinity sponge layer forcing:

```
s1 = npx.ones(settings.nz)*32
s2 = npx.ones(settings.nz)*32
s1 = s1.at[:12].set(npx.array([26, 26.5, 27, 27.5, 28, 28.5, 29, 29.5, 30, 30.5, 31, 31.5]))
s1 = npx.flip(s1)
s2 = s2.at[:6].set(npx.array([27, 28, 29, 30, 31, 32]))
s2 = npx.flip(s2)
s_array = npx.array([s1, s1, s2, s2])
day_in_seconds = 86400.0
(n1, f1), (n2, f2) = veros.tools.get_periodic_interval(vs.time, day_in_seconds*20, day_in_seconds*5, 4)
sss = update(vs.s_star, at[...], f1 * s_array[n1] + f2 * s_array[n2])
```

Sponge layer forcing restoring time: 2 hours

For case 5

Meridional wind stress: $\tau_y = 0$

Salinity sponge layer forcing:

```
s1 = npx.ones(settings.nz)*32
s2 = npx.ones(settings.nz)*36
s1 = s1.at[:13].set(npx.array([25.5, 26, 26.5, 27, 27.5, 28, 28.5, 29, 29.5, 30, 30.5, 31, 31.5]))
s1 = npx.flip(s1)
s2 = s2.at[:6].set(npx.array([33, 35, 36, 36, 36, 36]))
s2 = npx.flip(s2)
s_array = npx.array([s1, s2, s2])
day_in_seconds = 86400.0
(n1, f1), (n2, f2) = veros.tools.get_periodic_interval(vs.time, day_in_seconds*60, day_in_seconds*20, 3)
sss = update(vs.s_star, at[...], f1 * s_array[n1] + f2 * s_array[n2])
```

Sponge layer forcing restoring time: 2 hours

B Setup parameters

Setup	1	2	3	4	5	6	7	8
`A_h` $[\frac{m^2}{s}]$	1.0	10.0	10.0	10.0	10.0	10.0	10.0	10.0
`kappaM_min` $[\frac{m^2}{s}]$	$2 \cdot 10^{-4}$	$2 \cdot 10^{-4}$	$2 \cdot 10^{-4}$	$2 \cdot 10^{-4}$	$2 \cdot 10^{-4}$	$2 \cdot 10^{-4}$	$2 \cdot 10^{-4}$	$2 \cdot 10^{-4}$
`kappaH_min` $[\frac{m^2}{s}]$	$2 \cdot 10^{-5}$	$2 \cdot 10^{-5}$	$2 \cdot 10^{-5}$	$2 \cdot 10^{-5}$	$2 \cdot 10^{-5}$	$2 \cdot 10^{-5}$	$2 \cdot 10^{-5}$	$2 \cdot 10^{-5}$
`c_k`	0.1	0.1	0.1	0.1	0.3	0.1	0.1	0.1
`c_eps`	0.7	0.7	0.7	1.1	0.7	0.7	0.7	0.7
`K_iso_0` $[\frac{m^2}{s}]$	1.0	1.0	1.0	1.0	1.0	10.0	1.0	10.0
`K_iso_steep` $[\frac{m^2}{s}]$	1.0	1.0	1.0	1.0	1.0	10.0	1.0	10.0
`enable_noslip_lateral`	`False`	`False`	`False`	`False`	`False`	`False`	`True`	`True`

C Zonally averaged along fjord velocity for setup 2, 6, and 7

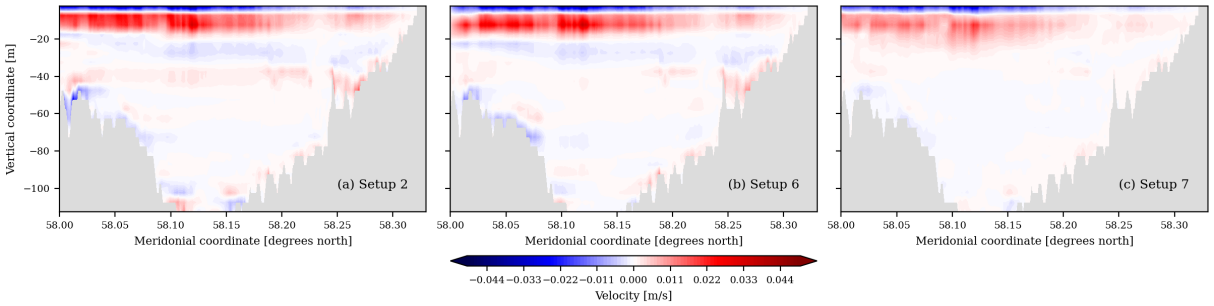

Figure 11: Zonally averaged along fjord velocity for (a): setup 2, (b): setup 6, (c): setup 7. Positive velocities are into the fjord and negative out of the fjord.

D Depth averaged noise

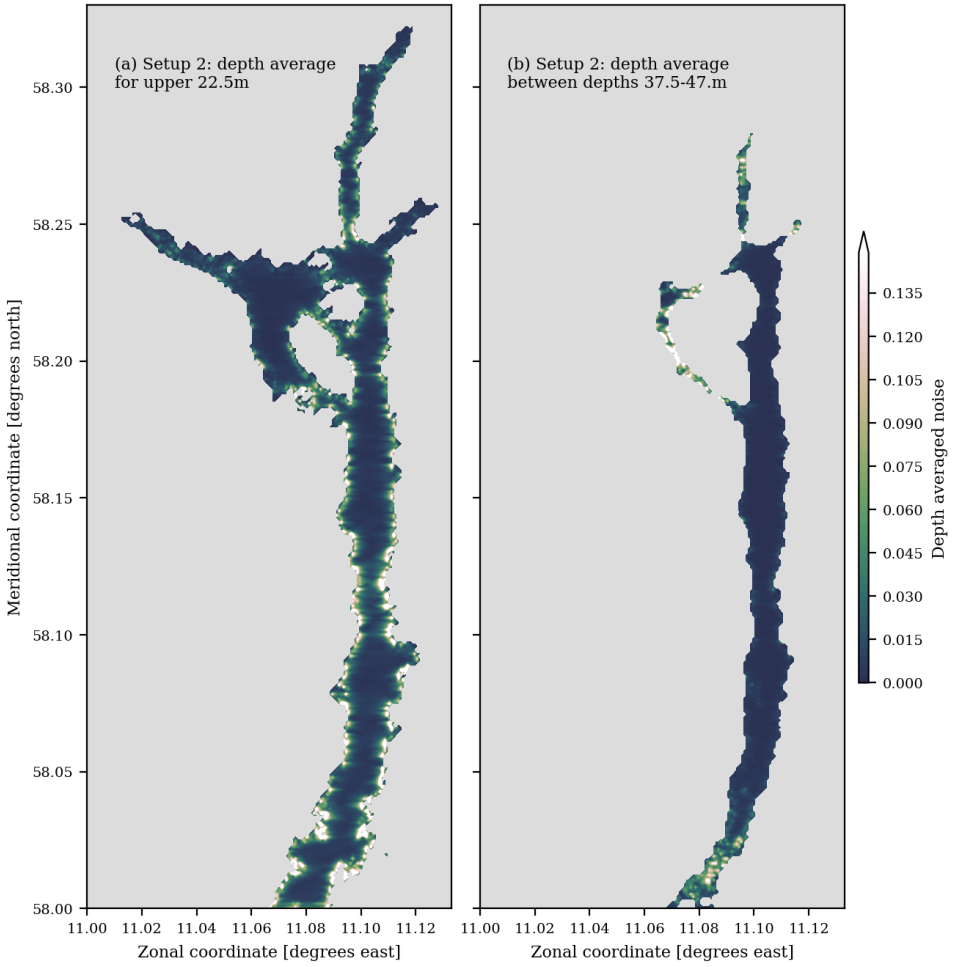

Figure 12: Depth averaged noise in setup 2 for (a): the upper 22.5 m, (b): between 37.5 m and 47.5 m

E Case 4: Location for Figure 9(a)

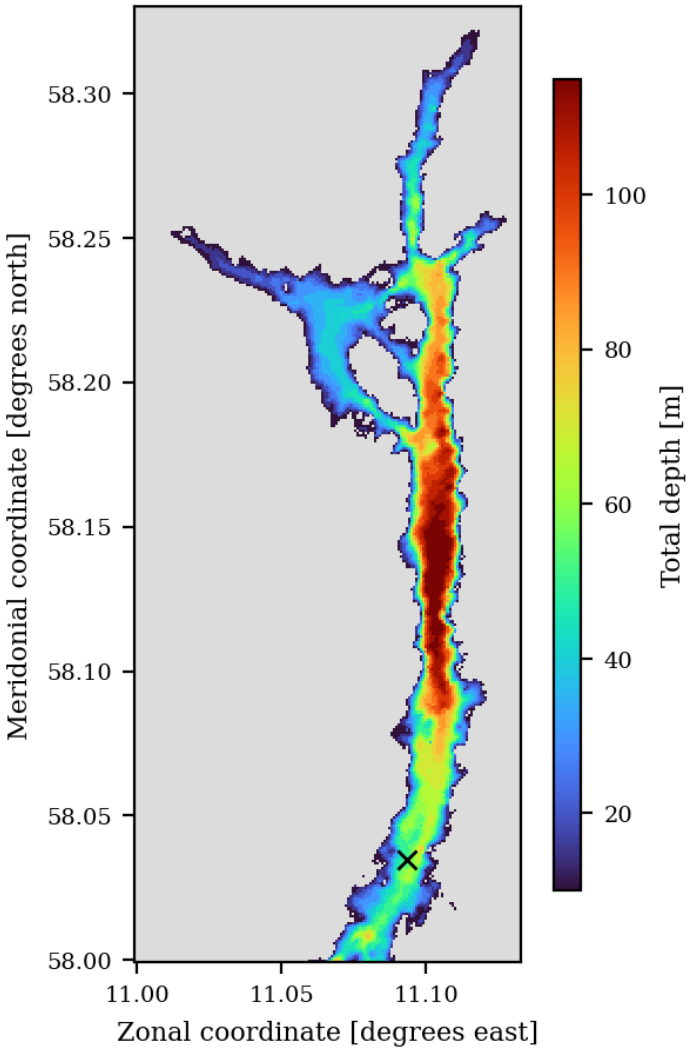

F Case 4: zonally averaged along fjord velocity for each day

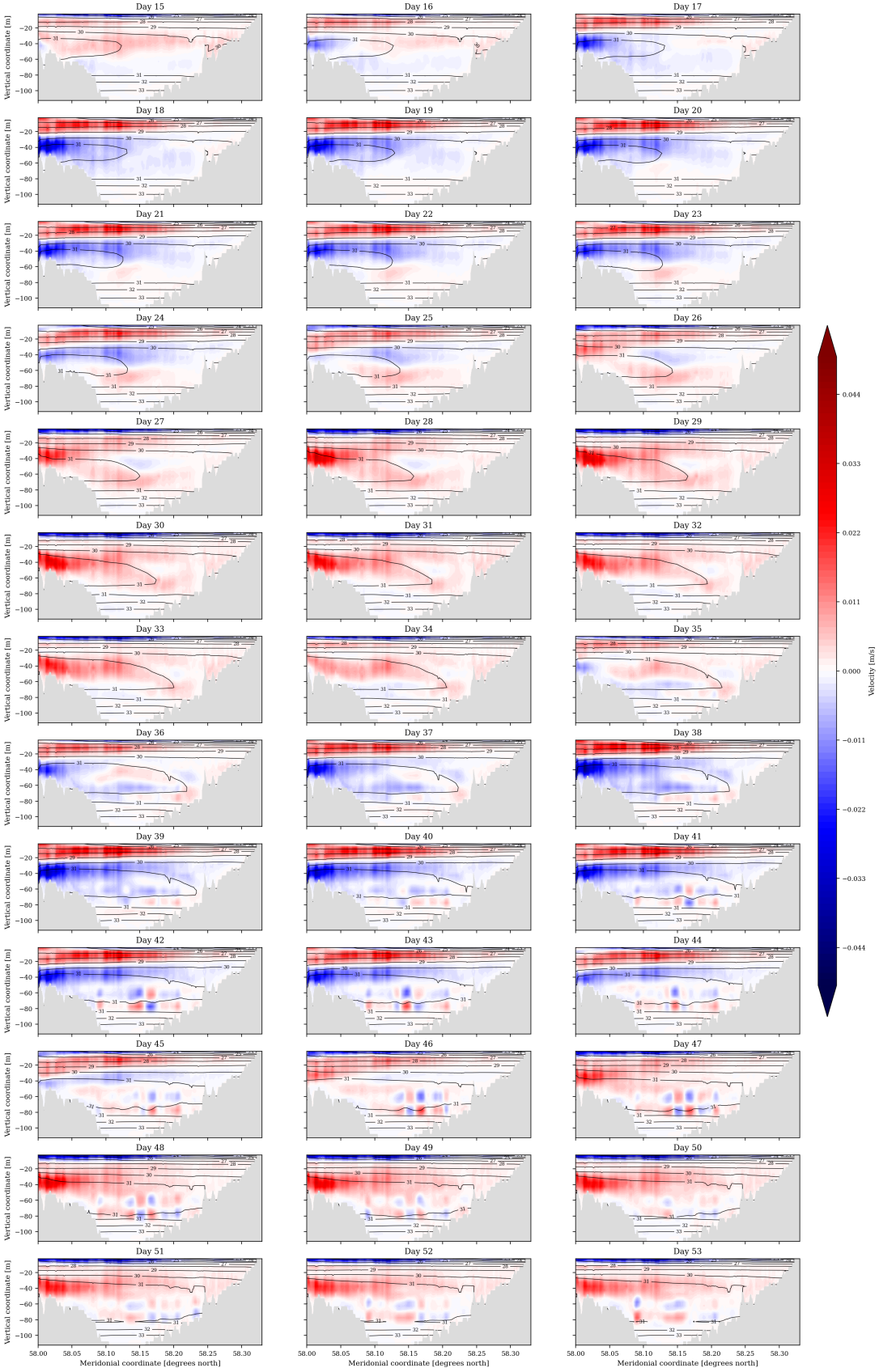

G Case 5: Location for Figure 10

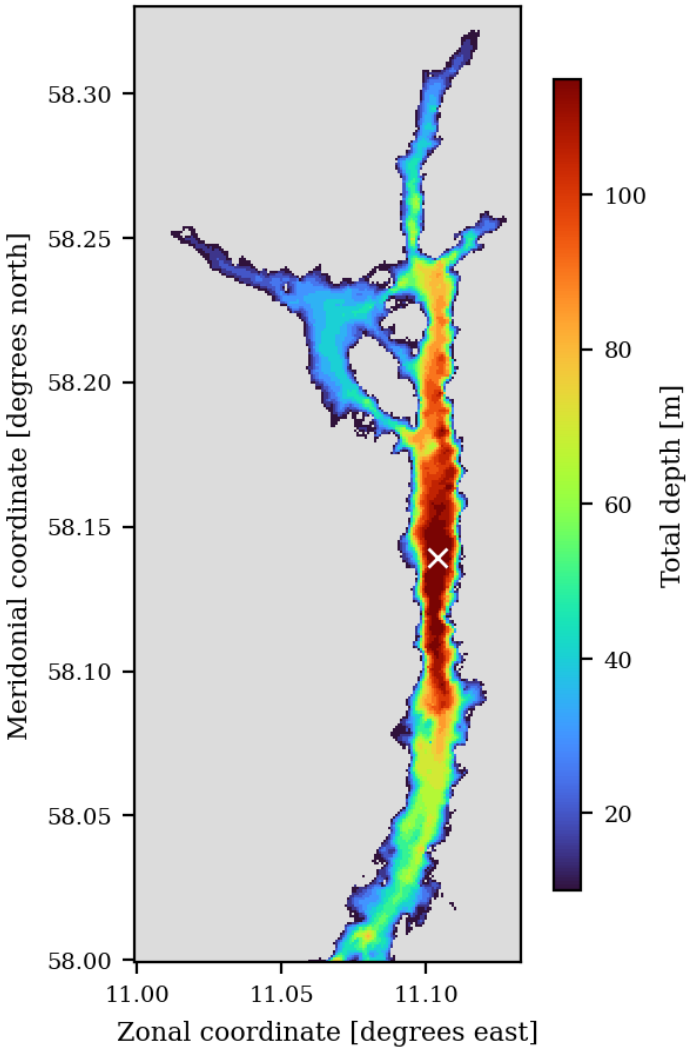

H Case 5: zonally averaged along fjord velocity for each day